Biomedical Engineering Advances 9 (2025) 100156

Contents lists available at ScienceDirect

Biomedical Engineering Advances

journal homepage: www.journals.elsevier.com/biomedical-engineering-advances

Decoding motor execution and motor imagery from EEG with deep learning and source localization

Sina Makhdoomi Kaviri, Ramana Vinjamuri *

Department of Computer Science and Electrical Engineering, University of Maryland Baltimore County, Baltimore, MD 21250, USA

ARTICLE INFO

Keywords:
Beamforming
Brain–computer interface
ResNet CNN
Source localization
Inverse problem

ABSTRACT

The use of noninvasive imaging techniques has become pivotal in understanding human brain functionality. While modalities like MEG and fMRI offer excellent spatial resolution, their limited temporal resolution, often measured in seconds, restricts their application in real-time brain activity monitoring. In contrast, EEG provides superior temporal resolution, making it ideal for real-time applications in brain–computer interface systems. In this study, we combined deep learning with source localization to classify two motor task types: motor execution and motor imagery. For motor imagery tasks—left hand, right hand, both feet, and tongue—we transformed EEG signals into cortical activity maps using Minimum Norm Estimation (MNE), dipole fitting, and beamforming. These were analyzed with a custom ResNet CNN, where beamforming achieved the highest accuracy of 99.15%, outperforming most traditional methods. For motor execution involving six types of reach-and-grasp tasks, beamforming achieved 90.83% accuracy compared to 56.39% from a sensor domain approach (ICA + PSD + TSCR-Net). These results underscore the significant advantages of integrating source localization with deep learning for EEG-based motor task classification, demonstrating that source localization techniques greatly enhance classification accuracy compared to sensor domain approaches.

1. Introduction

Electroencephalographic (EEG) signals are essential for brain–computer interfaces (BCIs), providing a non-muscular communication channel that particularly benefits individuals with severe neuromuscular disorders such as amyotrophic lateral sclerosis, brainstem stroke, and spinal cord injury. Advances in understanding brain function, along with improvements in computational capabilities and increasing needs in the disability community, have driven BCI research toward the development of innovative communication and control technologies [1]. Despite this progress, EEG research continues to face significant challenges due to the complexity of neurophysiological data and the lack of standardized analysis methods, underscoring the need for unified approaches [2]. Furthermore, the inherently noisy, low spatial resolution, and nonstationary characteristics of EEG signals make single-trial EEG classification difficult, thereby emphasizing the necessity for optimized classifier performance [3].

Several approaches have been developed to enhance motor imagery (MI) and motor execution (ME) classification. Recent work has explored filter bank common spatial pattern (FBCSP) with spiking neural networks (SNN) to improve multiple MI classification accuracy, achieving up to 90.09% accuracy [4]. A diverse feature fusion approach using brain functional connectivity (BFC) and FBCSP was also introduced to enhance MI classification, achieving an accuracy of 83.81% [5]. Moreover, a motor imagery-based virtual car control strategy demonstrated effective control with four MI classes, highlighting the feasibility of real-world MI-based applications [6]. Hybrid approaches combining EEG with functional near-infrared spectroscopy (fNIRS) have shown improvements of 5%–10% in MI classification accuracy by leveraging multimodal signals [7]. Additionally, deep learning models such as an improved dilation CapsuleNet (ID-CapsuleNet) have been explored for MI-based BCI, achieving high classification accuracies across multiple datasets [8]. These advancements highlight the need for further improvements in feature extraction, classification models, and multimodal fusion techniques for MI and ME decoding.

To fully utilize the potential of EEG in BCIs, researchers have explored various applications. Motor behavior studies have differentiated sustained and movement phase-related EEG amplitudes, revealing distinct networks for different motor functions [9]. EEG has also predicted driving actions for advanced driver-assistance systems [10]. Studies on individuals with spinal cord injury showed potential for EEG-based BCIs in regaining motor functions [11]. Systems neuro-engineering is evolving to integrate neuroimaging, neural interfacing, and neuromodulation for advanced neuro-devices [12]. Electrophysiological source

* Corresponding author.
E-mail address: rvinjam1@umbc.edu (R. Vinjamuri).

https://doi.org/10.1016/j.bea.2025.100156
Received 19 December 2024; Received in revised form 10 March 2025; Accepted 12 March 2025
Available online 22 March 2025
2667-0992/© 2025 The Authors. Published by Elsevier Inc. This is an open access article under the CC BY-NC-ND license (http://creativecommons.org/licenses/by-nc-nd/4.0/).

imaging (ESI) with multimodal neuroimaging improves brain activity mapping [13]. Recent BCI advancements include controlling prosthetic limbs with multiple degrees of freedom in Ref. [14] and using conditional Generative Adversarial Networks (cGANs) for generating target and non-target images from EEG epochs [15].

To address these challenges, researchers have explored various classification algorithms for EEG analysis. A review reveals diverse approaches, including linear classifiers, neural networks, and classifier combinations. Support Vector Machines (SVMs) show efficacy in synchronous BCIs due to their regularization properties, though standardized comparisons between classifiers are lacking. General-purpose BCI systems like BCI2000 and Open-ViBE facilitate standardized testing [16]. Incorporating goal-directed movements in BCI applications enhances movement intention classification, using motor and parietal area neural activity [17]. Moreover, deep learning methods, particularly convolutional and recurrent learning, have improved brain state classification and diagnosis of conditions like Alzheimer's disease [18]. A review of 154 papers on DL applied to EEG data highlighted trends, challenges, and the advantages of using DL for EEG classification, while emphasizing the need for large datasets to fully exploit DL's potential [19]. In response to the need for high-resolution spatiotemporal neuroimaging, a novel framework for fMRI–EEG integrated cortical source imaging is presented, enhancing source localization and waveform estimation [20]. Integrating deep learning with EEG has revolutionized brain activity analysis, improving diagnostic and therapeutic interventions [21].

Decoding upper limb movements using low-frequency EEG signals has achieved significant classification accuracies, with some studies reporting over 90%, crucial for developing non-invasive control strategies for neuro-prostheses or robotic arms [22]. Neural interface systems have allowed individuals with tetraplegia to control robotic arms for complex movements, showing the potential of BCIs [23]. Deep learning and time-frequency analysis of EEG signals have reached high accuracy, with one study achieving 90.3% accuracy in distinguishing premovement from resting phases and 62.47% in discriminating different motor preparations [24]. A deep CNN approach showed up to 90.50% accuracy in classifying hand sub-movements versus resting state, identifying key cortical areas involved in motor preparation [25].

In this paper, we introduce a novel approach for classifying motor tasks using EEG data from two distinct datasets: one focused on four-class classification involving left hand, right hand, both feet, and tongue movements, and another concentrating on six reach-and-grasp tasks. Our methodology leverages advanced source localization techniques, including MNE, dipole fitting, and beamforming, to enhance the spatial resolution of EEG signals. Additionally, we developed a customized ResNet CNN architecture designed to effectively capture and classify the spatial patterns present in source-localized EEG data.

The application of source localization significantly improved the classification accuracy by transforming EEG data from the sensor to the source domain, providing a more precise representation of cortical activity. For instance, this approach improved classification accuracies for reach and grasp motor tasks, achieving an average test accuracy of 90.83% with beamforming, 84.10% with MNE, and 81.32% with dipole fitting, compared to 56.39% without source localization. Beamforming, in particular, enhanced precision from 41.79% in the sensor domain to between 85.00% and 98.55% in the source domain. Our customized ResNet CNN model achieved F1-scores of 90.85% with source localization, compared to significantly lower scores in the sensor domain, highlighting the critical role of accurate spatial mapping in EEG analysis.

The main contributions of this paper include:

(i) **Comprehensive methodology**: An integrated approach combining advanced preprocessing, source localization, and deep learning techniques, significantly enhancing classification accuracy and reliability for both four-class and reach-and-grasp tasks.

(ii) **Efficacy in source localization**: The demonstration of multiple source localization techniques (MNE, dipole fitting, beamforming) to reconstruct cortical sources, providing a detailed and spatially accurate view of cortical activity, which is crucial for decoding complex motor tasks.

(iii) **Robust ResNet CNN architecture**: A customized ResNet CNN architecture incorporating sensitivity analysis and early stopping mechanisms, improving robustness and accuracy in classifying motor tasks across different EEG datasets.

The rest of the paper is organized as follows: Section 2 describes the *Methodology*, including the system description, data details, preprocessing, source localization, ResNet CNN architecture, system setup, and the advanced feature extraction and classification methodology. Section 3 presents the *Results and Discussions*, detailing the classification performance with and without source localization, and the effectiveness of different source localization techniques in enhancing EEG analysis. Section 4 concludes the paper, summarizing key findings and suggesting directions for future research.

2. Methodology

2.1. System description

This study focuses on classifying motor tasks using EEG data by integrating advanced signal processing and deep learning techniques. The overall framework is illustrated in Fig. 1. EEG data were recorded from subjects performing grasp and motor imagery tasks, with source localization methods applied to improve spatial resolution. The extracted cortical activity features were subsequently classified using a deep learning framework. For the six-task grasp classification, EEG signals were recorded using a high-density 32-electrode EEG cap, capturing neural activity from motor-related brain regions. Each trial lasted for 8 s, consisting of a pre-movement phase followed by a reach-grasp-hold phase. The preprocessing pipeline included band-pass filtering (0.01–200 Hz) for noise reduction, a 50 Hz notch filter to remove power line interference, and downsampling to 256 Hz for computational efficiency. To reconstruct cortical sources associated with motor execution, source localization techniques such as MNE, dipole fitting, and beamforming were applied. The extracted features were fed into a ResNet CNN for classification, as illustrated in Fig. 1.

For the four-task motor imagery classification, the experimental design followed a structured trial sequence, as depicted in Fig. 2. Each trial began with an auditory beep, followed by a fixation cross at 2 s and a cue at 3 s, prompting the subject to perform a motor imagery task from 3 to 6 s. The trial concluded with a break period between 6 and 8 s. EEG signals were recorded using 22 electrodes placed over motor-related cortical areas, capturing neural activity specific to left hand, right hand, feet, and tongue imagery tasks. Preprocessing steps included constructing the forward model, computing the lead field matrix, and selecting relevant time windows for solving the inverse problem. These spatially enhanced features were then classified using a ResNet CNN. This methodology integrates structured EEG acquisition, systematic preprocessing, advanced source localization, and deep learning techniques to improve classification accuracy across both grasp and motor imagery tasks.

2.2. Data description

This study utilizes two EEG datasets to classify motor tasks based on source-localized EEG signals. The first dataset consists of recordings from 10 right-handed subjects performing six distinct grasp tasks, each repeated 30 times. Data collection was conducted under an approved protocol by the Institutional Review Board (IRB) of Stevens Institute of Technology. Each trial lasted for 8 s, comprising a 4-second pre-movement phase followed by a 4-second reach-grasp-hold

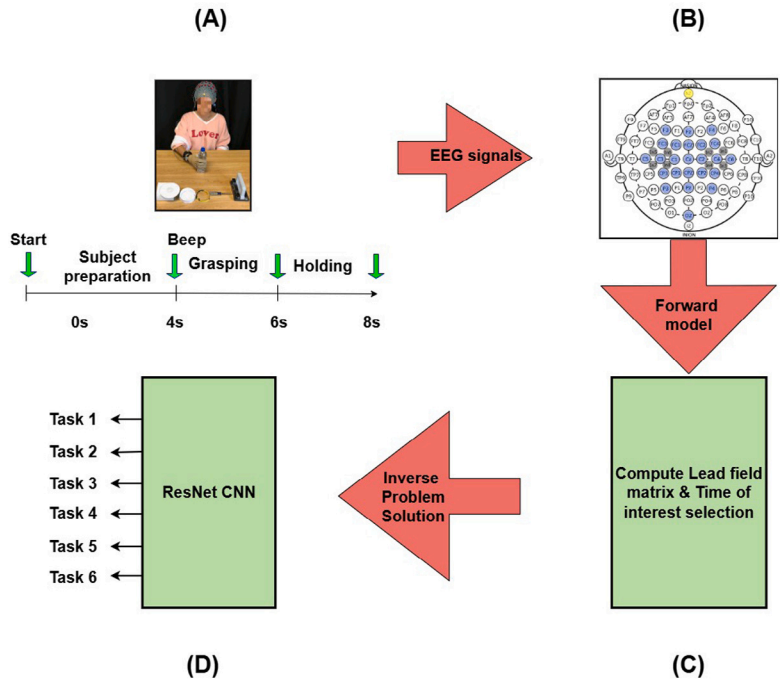

Fig. 1. Proposed framework for EEG-based task classification of grasping activities. (A) Trial timing illustration: subject preparation followed by an auditory cue (beep) at 4 s, initiating grasping between 4 to 6 s, and holding from 6 to 8 s. The image shows a participant with an EEG cap performing the task. (B) The forward model development using EEG signals recorded from high-density electrodes, which represent activity over key brain regions. (C) The lead field matrix computation and time of interest selection are part of preprocessing for source localization. (D) A ResNet CNN architecture is employed for classifying six grasping-related tasks based on the inverse problem solutions obtained from the forward model.

phase. The EEG signals were recorded at a 256 Hz sampling rate, resulting in 2048 samples per trial, with 32 active electrodes capturing neural activity. The EEG recordings were synchronized with hand kinematics data obtained using a CyberGlove to accurately track motor actions [26]. The CyberGlove (CyberGlove Systems LLC, San Jose, CA, USA) recorded finger movements by measuring joint angles, including the metacarpophalangeal (MCP) joints of the thumb and fingers, the interphalangeal (IP) joint of the thumb, and the proximal interphalangeal (PIP) joints of the four fingers. This data was sampled at 125 Hz using a custom-built LabVIEW interface, which also provided auditory cues and synchronized EEG and motion data. EEG recordings were obtained using a high-density EEG cap (g.GAMMA cap, g.tec, Schiedlberg, Austria) with 32 electrodes following the 10–20 system. The electrode placement covered frontal, central, parietal, and occipital regions, with electrodes positioned at F3, Fz, F4, FC3, FC1, FCz, FC2, FC4, C5, C3, C1, Cz, C2, C4, C6, CP3, CP1, CPz, CP2, CP4, P3, Pz, P4, and Oz, along with eight intermediate sites, as shown in Fig. 1 [26].

The second dataset, originally published as Dataset 2a in 2008, consists of EEG recordings from 9 subjects performing a cue-based BCI paradigm involving four motor imagery tasks: left hand, right hand, both feet, and tongue. Each subject completed two sessions recorded on separate days. Each session contained 6 runs, with each run comprising 48 trials (12 trials per class), resulting in a total of 288 trials per session [27]. To estimate and correct eye movement artifacts, each session began with a 5-minute EOG recording divided into three segments: two minutes with eyes open, one minute with eyes closed, and one minute of directed eye movements. EEG signals were captured using 22 Ag/AgCl electrodes positioned according to the international 10–20 system, with an additional three monopolar EOG channels to monitor ocular activity. The data were sampled at 250 Hz and band-pass filtered between 0.5 Hz and 100 Hz, with a 50 Hz notch filter applied to remove power line noise. Trials containing artifacts were visually inspected by an expert and labeled accordingly. This dataset provides a well-established benchmark for evaluating artifact removal techniques and motor imagery classification models [27] (see Table 1).

Table 1
Summary of the experimental setup for the two EEG datasets used in this study.

Feature	Reach and grasp dataset	Dataset 2a (Motor imagery)
Number of subjects	10	9
Number of tasks	6 (Grasp Types)	4 (Left Hand, Right Hand, Feet, Tongue)
Trials per task	30	288 (per session)
Sessions per subject	1	2 (recorded on separate days)
Trial duration	8s (4s pre-movement + 4s grasp-hold)	8s (2s fixation, 1s cue, 3s imagery, 2s break)
Sampling rate	256 Hz	250 Hz
Number of electrodes	32	22 (plus 3 EOG channels)
Electrode placement	10-20 System (frontal, central, parietal, occipital)	10-20 System
Artifact removal	Visual Inspection, Filtering	Visual Inspection, EOG-based correction
Additional sensors	CyberGlove (hand kinematics)	Eye movement tracking (EOG)

2.3. Preprocessing

Preprocessing was performed separately for each dataset to ensure optimal data quality and improve classification performance.

2.3.1. Grasp task EEG preprocessing:

The preprocessing pipeline for the grasp task dataset involved multiple steps to enhance signal quality before source localization and classification:

- **Band-Pass Filtering:** A finite impulse response (FIR) band-pass filter (0.01–200 Hz) was applied to remove low-frequency drifts and high-frequency noise.

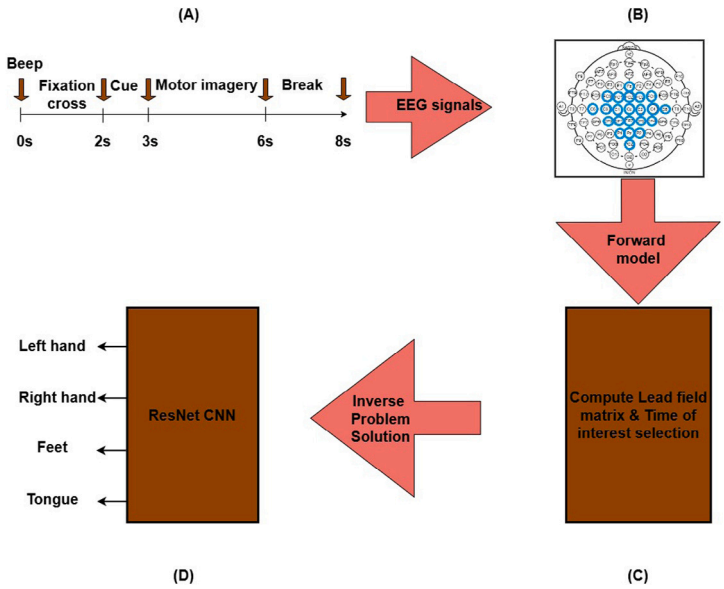

Fig. 2. Framework for motor imagery classification involving four tasks. (A) Trial timing details: an auditory beep initiates the trial, followed by a fixation cross at 2 s, cue presentation at 3 s, motor imagery execution from 3 to 6 s, and a break period from 6 to 8 s. (B) EEG data acquisition using 22 active electrodes positioned to capture key cortical regions. (C) Data preprocessing steps include the forward model construction, lead field matrix computation, and time of interest selection to facilitate inverse problem-solving for source localization. (D) A ResNet CNN is applied for classification of four motor imagery tasks, including left hand, right hand, feet, and tongue, utilizing features derived from source-localized signals.

- **Notch Filtering:** A 50 Hz notch filter was used to eliminate power line interference.
- **Downsampling:** The EEG signals were downsampled from their original sampling rate to 256 Hz for computational efficiency while preserving task-related neural activity.
- **Epoch Selection:** EEG trials were segmented into 8-second epochs, with a focus on the pre-movement and reach-grasp-hold phases.
- **Source Localization:** MNE, dipole fitting, and beamforming were applied to reconstruct cortical sources, enhancing spatial resolution before feature extraction.

2.3.2. Motor imagery EEG preprocessing:

The preprocessing steps for the motor imagery dataset were tailored to extract discriminative features for classification:

- **Band-Pass Filtering:** EEG signals were filtered within the range of 0.5–100 Hz to retain motor-related frequency components while removing slow drifts and high-frequency noise.
- **Notch Filtering:** A 50 Hz notch filter was applied to remove electrical interference.
- **Epoch Selection:** EEG trials were segmented into 8-second epochs, focusing on the motor imagery phase (3 to 6 s) to capture task-related neural activity.
- **Artifact Removal:** Eye movement artifacts were identified using the EOG recordings and removed through Independent Component Analysis (ICA).
- **Source Localization:** The forward model and lead field matrix were computed to perform source reconstruction, improving the spatial specificity of neural activity.

These preprocessing pipelines ensured that the EEG signals were optimized for classification, reducing noise and enhancing the separability of motor tasks in the feature space. The resulting source-localized signals were then used as input to the ResNet CNN model for accurate task classification.

2.4. Source localization and inverse problem

EEG provides high temporal resolution for monitoring brain activity but has poor spatial resolution due to volume conduction, where electrical activity generated at different cortical sources mixes at the scalp electrodes. To overcome this limitation, source localization techniques such as MNE, dipole fitting, and beamforming were employed to reconstruct cortical activity from EEG signals. These methods require solving the inverse problem using a forward model that describes how neural current sources generate EEG scalp potentials.

2.4.1. Forward model:

The forward model mathematically relates cortical sources to observed EEG signals and is expressed as:

$$\mathbf{x}(t) = \mathbf{L}\mathbf{q}(t) + \mathbf{n}(t) \tag{1}$$

where:

- $\mathbf{x}(t) \in \mathbb{R}^{M\times 1}$ represents the EEG measurements at M electrodes at time t,
- $\mathbf{L} \in \mathbb{R}^{M\times N}$ is the lead field matrix, which describes the mapping between N neural sources and EEG sensors,
- $\mathbf{q}(t) \in \mathbb{R}^{N\times 1}$ denotes the unknown current sources at N locations in the brain,
- $\mathbf{n}(t)$ accounts for noise and artifacts.

The lead field matrix $\mathbf{L}$ was computed using the New York Head (NYH) forward model [28], a realistic head model that incorporates tissue conductivity properties. Constructing the forward model involves:

- defining head tissue conductivities (scalp, skull, cerebrospinal fluid, and brain),
- selecting a source space within the cortical volume,
- mapping source activations to electrode potentials.

Once the forward model is established, the inverse problem is solved to estimate cortical sources from EEG recordings.

2.4.2. Inverse problem and regularization techniques:

The inverse problem aims to recover $\mathbf{q}(t)$ given EEG measurements $\mathbf{x}(t)$. Since the number of possible sources exceeds the number of electrodes ($N \gg M$), the problem is unstable, requiring regularization techniques to obtain physiologically meaningful solutions.

Dipole Fitting: This method assumes that brain activity originates from a small number of equivalent current dipoles. The optimal dipole locations $\mathbf{r}$ and moments $\mathbf{q}(t)$ are estimated by minimizing: [29]

$$\hat{\mathbf{r}}, \hat{\mathbf{q}}(t) = \arg\min_{\mathbf{r},\mathbf{q}(t)} \|\mathbf{x}(t) - \mathbf{L}(\mathbf{r})\mathbf{q}(t)\|^2 \tag{2}$$

where $\mathbf{L}(\mathbf{r})$ is the lead field matrix evaluated at dipole locations. Dipole fitting provides high spatial resolution but assumes focal activity.

MNE: MNE finds the source configuration with minimal energy while maintaining consistency with EEG data. The cost function is: [30]

$$\hat{\mathbf{q}}(t) = \arg\min_{\mathbf{q}(t)} \|\mathbf{x}(t) - \mathbf{L}\mathbf{q}(t)\|^2 + \lambda \|\mathbf{q}(t)\|^2 \tag{3}$$

where:

- $\|\mathbf{x}(t) - \mathbf{L}\mathbf{q}(t)\|^2$ ensures consistency with EEG data,
- $\lambda \|\mathbf{q}(t)\|^2$ imposes smoothness on source activations,
- λ is the regularization parameter.

MNE is widely used for distributed source estimation but tends to produce blurred solutions.

Beamforming: Beamforming constructs spatial filters to isolate specific neural sources while suppressing background noise. The estimated sources are computed as: [31]

$$\hat{\mathbf{q}}(t) = \mathbf{W}\mathbf{x}(t) \tag{4}$$

where $\mathbf{W}$ is the beamforming filter:

$$\mathbf{W} = (\mathbf{L}^T\mathbf{C}_x^{-1}\mathbf{L} + \lambda\mathbf{I})^{-1}\mathbf{L}^T\mathbf{C}_x^{-1} \tag{5}$$

Here, $\mathbf{C}_x$ is the EEG covariance matrix and λ is a regularization term. Beamforming improves spatial resolution by dynamically suppressing interference.

2.4.3. Application to EEG data:

EEG signals were recorded using 32 electrodes for the first dataset and 22 electrodes (plus 3 EOG channels) for the second dataset. The forward model was applied to these signals, and the inverse problem was solved using MNE, dipole fitting, and beamforming. Each method provided distinct advantages:

- Dipole fitting achieved precise localization for focal sources.
- MNE produced distributed source estimates with smooth activations.
- Beamforming enhanced spatial resolution by isolating individual sources.

The reconstructed cortical sources served as inputs to the deep learning model, allowing for improved EEG-based classification of motor tasks.

2.5. ResNet architecture for EEG classification

The ResNet architecture was designed to classify EEG-based motor tasks for two different datasets. ResNet CNN was chosen over EEGNet due to its deeper architecture, which enables better feature extraction and hierarchical learning of spatial and temporal EEG patterns. Unlike EEGNet, which is optimized for lightweight architectures with depthwise and separable convolutions, ResNet employs residual connections that mitigate the vanishing gradient problem, allowing for effective training of deeper networks. This is particularly beneficial for EEG data, where capturing complex spatial–temporal dependencies is crucial for improving classification performance. Additionally, ResNet CNN has demonstrated robustness in handling subject variability and noise, making it a more suitable choice for our dataset.

The input data for the first dataset consists of six grasp tasks, structured as 180 trials (30 trials per task) with each trial comprising 256 time samples, corresponding to the EEG sampling rate of 256 Hz. For the second dataset, which involves four-class motor imagery tasks (left hand, right hand, both feet, and tongue), the ResNet model was adapted with a modified output layer containing four neurons instead of six.

2.5.1. Convolutional and pooling layers:

The architecture begins with a 2D Convolutional Layer (Conv2D) that applies learnable filters across EEG spatial and temporal dimensions. These convolutional filters extract spatial dependencies across electrodes while preserving temporal patterns within trials. Batch Normalization follows to stabilize training, and a ReLU activation function introduces non-linearity, allowing the model to capture complex patterns.

A Max Pooling (MaxPool2D) layer is incorporated to reduce the dimensionality of feature maps while preserving essential spatial and temporal information. This pooling operation minimizes computational cost and prevents overfitting by discarding irrelevant variations in EEG signals.

2.5.2. Inception blocks for multi-scale feature extraction:

To improve feature extraction across multiple spatial and temporal scales, the model integrates Inception blocks. These blocks use different convolutional filter sizes (e.g., 1×1, 3×3, and 5×5) to capture short-term and long-term dependencies simultaneously. The combination of multiple kernel sizes ensures that both localized and distributed EEG patterns are learned effectively.

2.5.3. Residual blocks for efficient training:

Residual connections are employed to facilitate gradient flow during backpropagation. Standard deep networks suffer from vanishing gradients, leading to inefficient learning as depth increases. Residual blocks mitigate this issue by incorporating skip connections:

$$\mathbf{y} = \mathcal{F}(\mathbf{x}) + \mathbf{x} \tag{6}$$

where $\mathcal{F}(\mathbf{x})$ represents the transformation applied by a sequence of convolutional layers, and the input $\mathbf{x}$ is directly added to the output. This design allows the model to retain essential features from earlier layers, improving convergence and classification accuracy.

2.5.4. Attention mechanism for feature enhancement:

To further refine feature selection, Attention blocks are incorporated into the model. These blocks enhance task-relevant EEG components while suppressing background noise. The attention mechanism assigns higher weights to informative time segments and spatial locations, improving robustness against inter-subject variability.

2.5.5. Global average pooling and fully connected layers:

Following hierarchical feature extraction, a Global Average Pooling (GAP) layer aggregates spatial feature maps into a single vector, significantly reducing the number of trainable parameters while maintaining task-relevant information. The resulting vector is passed through two fully connected layers with 512 and 256 neurons, followed by the final classification layer.

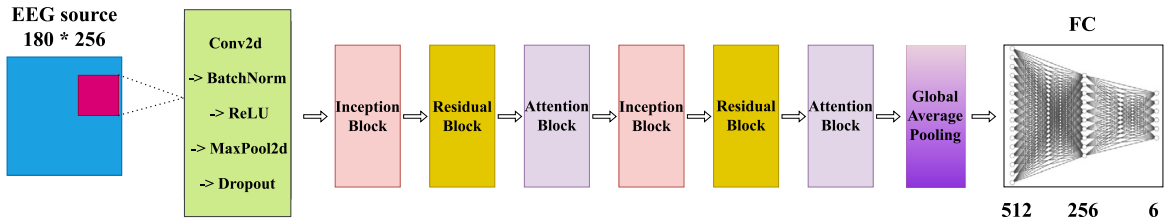

Fig. 3. Architecture of the proposed ResNet for classification of six reach and grasp tasks. The architecture starts with a convolutional layer followed by Batch Normalization, ReLU nonlinearity, Max Pooling, and Dropout layers. It then incorporates a sequence of Inception blocks, Residual blocks, and Attention blocks to extract spatial and feature hierarchies from the EEG source data. The network concludes with a Global Average Pooling layer to reduce the feature maps to a vector of class scores, which is further processed through fully connected (FC) layers with hidden sizes of 512 and 256, ending with a final output layer containing six units corresponding to the classification of the six distinct reach and grasp tasks.

2.5.6. Training strategy and optimization:

For both datasets, the model was trained using the Adam optimizer with a learning rate of:

$$\alpha = 10^{-2} \tag{7}$$

and exponential decay parameters:

$$\beta_1 = 0.9, \quad \beta_2 = 0.99 \tag{8}$$

Stratified K-Fold cross-validation was implemented to ensure robust performance across subjects. Training was stopped when validation accuracy stopped improving to avoid overfitting. The architecture of the proposed ResNet, as presented in Fig. 3, showcases significant potential for applications in biomedical signal processing.

2.6. System setup

The ResNet CNN was implemented using PyTorch, which offers flexibility and dynamic computational graph capabilities. Training was performed on an Alienware Aurora R16 system equipped with a 13th Gen Intel Core i9-13900F CPU @ 2.00 GHz, 32 GB of RAM, and an NVIDIA GeForce RTX 4070 SUPER GPU with 12 GB of GDDR6X memory. This high-performance setup enabled efficient training and fine-tuning of the deep learning model, ensuring optimal classification accuracy for EEG motor imagery tasks. To analyze neural activity for motor tasks, we performed source localization and time-frequency analysis of EEG data using the FieldTrip toolbox [32].

2.7. Advanced feature extraction and classification methodology

In this study, we aimed to decode motor tasks from two distinct EEG datasets: one involving four motor imagery tasks (left hand, right hand, both feet, and tongue) and another focusing on various reach and grasp tasks. The analysis pipeline involved detailed preprocessing, source localization, and deep learning techniques to extract relevant features and accurately classify motor activities.

The initial step of our analysis included preprocessing the EEG data. This step was crucial for removing artifacts, such as eye blinks and muscle movements, thereby retaining only meaningful signals that were critical for motor task classification. Once the EEG data were cleaned, the signals were segmented based on specific task events, focusing specifically on time windows surrounding the movement onset to capture relevant neural dynamics. We also concentrated on electrodes related to Brodmann areas 4 and 6 regions associated with motor planning and execution.

To solve the inverse problem of EEG source localization, we employed three advanced source localization techniques such as Dipole Fitting, MNE, and Beamforming. These techniques allowed us to reconstruct cortical activity for specific time windows associated with motor tasks, providing insights into the spatial dynamics of motor execution. By localizing these cortical sources, we focused on key motor regions such as the primary motor cortex (M1) and premotor cortex (PMC), essential for motor planning and execution during grasp-related activities.

The reconstructed EEG sources were then used as inputs to a customized ResNet-CNN to classify the different motor tasks. Incorporating the spatial information from source localization provided the network with enhanced features, leading to improved classification performance compared to traditional sensor-level analysis. The data was split into training (60%), validation (20%), and testing (20%) sets to ensure a robust evaluation of the model while minimizing overfitting risks. This detailed approach allowed us to achieve a higher classification accuracy and understand the spatial and temporal brain dynamics associated with each motor task.

Fig. 4 illustrates the EEG segments for six reach-and-grasp tasks, averaged across multiple trials and focusing on key electrodes that correspond to Brodmann Areas 4 and 6, which are responsible for motor function. The figure presents the EEG activity across the electrodes C3, C4, Cz, FC1, and FC2 for each task. These electrodes were chosen as they are critical for understanding motor control and are typically associated with activity in the motor and premotor areas.

The figure provides a detailed view of the neural dynamics associated with each grasp task:

- **Screwdriver Task (Cylindrical or Tripod Grasp)**:
  - Distinct activation patterns at electrodes C3 and C4.
  - Increased activity around movement onset, indicating motor cortex engagement.
  - Reflects contralateral motor control involvement.
- **Water Bottle Task (Cylindrical Grasp)**:
  - Marked neural activation at electrode Cz.
  - Involvement of the primary motor cortex (M1) and supplementary motor area (SMA).
  - Crucial for gross motor coordination and stabilization during the grasp.
- **CD Task (Lateral Key Grasp)**:
  - Localized activity around electrodes FC1 and FC2.
  - Involvement of the premotor cortex (PMC), engaged during fine motor control tasks.
  - Specific to lateral grasping activities.
- **Petri Dish Task (Spherical Grasp)**:
  - Widespread activation observed at FC1 and Cz.
  - Reflects the recruitment of the posterior parietal cortex (PPC).
  - PPC plays a key role in spatial awareness during spherical grasps.
- **Handle Task (Hook Grasp)**:
  - Significant response at electrode Cz.

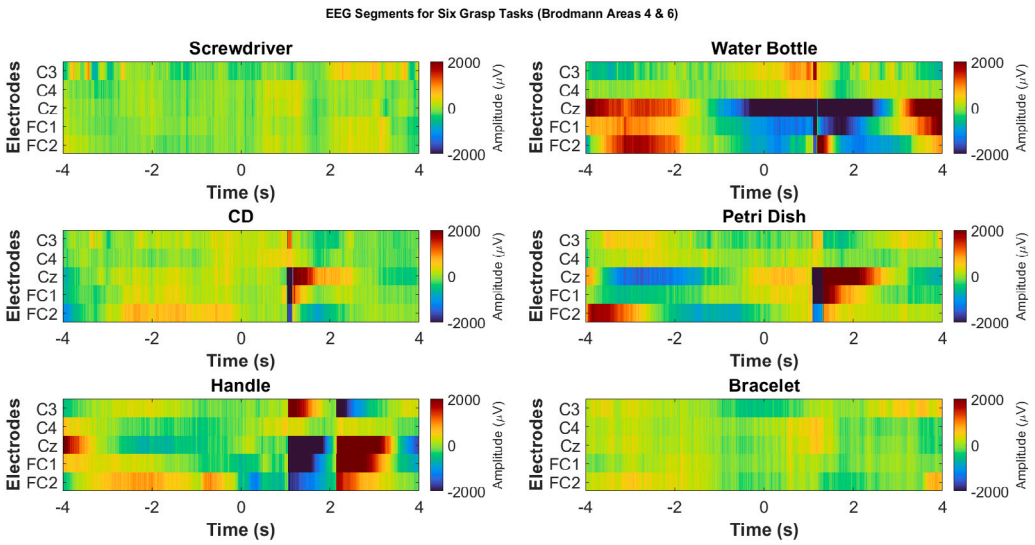

Fig. 4. EEG segments for six reach-and-grasp tasks. Each subfigure represents the EEG activity across specific electrodes (C3, C4, Cz, FC1, FC2) associated with Brodmann Areas 4 and 6 for each task. The tasks are arranged in three rows and two columns: (top row, from left to right) Screwdriver (cylindrical or tripod grasp), Water Bottle (cylindrical grasp); (middle row, from left to right) CD (lateral key grasp), Petri Dish (spherical grasp); (bottom row, from left to right) Handle (hook grasp), Bracelet (pinch or precision grasp). Time is represented on the x-axis from −4 to 4 s, where zero denotes movement onset. The y-axis indicates the electrode, and color represents EEG amplitude in microvolts (μV).

  - Reflects the role of the motor cortex in managing grip stability and strength.

- **Bracelet Task (Pinch or Precision Grasp)**:

  - High neural activation across electrodes C3 and FC2.
  - Indicates the involvement of the anterior intraparietal sulcus (aIPS) and M1.
  - Crucial for coordinating precision movements.

In addition, Fig. 5 depicts the EEG segments for four motor imagery tasks, averaged across multiple trials and focusing on key electrodes corresponding to Brodmann Areas 4 and 6, which are associated with motor planning and execution. The figure represents neural activity recorded from electrodes C3, C4, Cz, FC1, and FC2, which play a crucial role in decoding motor imagery tasks.

The figure provides a concise representation of the temporal dynamics observed during different imagined movements:

- **Left Hand Imagery**: Increased activation in C3, indicative of contralateral motor cortex involvement.
- **Right Hand Imagery**: Enhanced neural responses in C4, reflecting motor-related activity specific to right-hand movements.
- **Feet Imagery**: Pronounced activity in central electrodes, particularly Cz, highlighting engagement of the primary motor cortex.
- **Tongue Imagery**: Distributed activation patterns with notable responses in FC1 and FC2, corresponding to cortical regions responsible for orofacial motor control.

Finally, the use of source localization techniques such as Dipole Fitting, MNE, and Beamforming allowed us to identify neural sources involved in reach and grasp actions, providing insights into the specific brain regions activated during these tasks. These localized sources were used as input features for a ResNet CNN, significantly improving classification accuracy compared to using raw EEG data alone. The enhanced understanding of unique activation patterns for each grasp type contributes to developing better motor rehabilitation strategies and BCIs by leveraging motor cortical dynamics. Additionally, time-frequency analysis of the source-localized data highlighted crucial frequency bands, such as beta, essential for motor control. This study presents an effective methodology that integrates source localization, deep learning, and careful data preprocessing, advancing EEG-based motor decoding.

The brain activation patterns observed during motor imagery tasks for the left hand, right hand, feet, and tongue provide critical insights into the involvement of specific regions within the motor cortex, particularly Brodmann areas 4 and 6. Using beamforming techniques, the results indicate how different body parts activate distinct areas in the motor cortex, adhering to the **somatotopic organization** of the brain which refers to the structured mapping of body parts within the motor cortex, where distinct cortical areas are responsible for controlling specific movements. These distinct activations are represented in Fig. 6, showcasing the differential engagement of the motor cortex across various tasks. The following discussion breaks down each motor imagery task:

For left hand motor imagery, the activation predominantly occurs in the right hemisphere, particularly in the hand region of the primary motor cortex (Brodmann area 4), as shown in Fig. 6a. The premotor cortex (Brodmann area 6) is also involved, indicating motor planning processes necessary for simulating fine motor control of the left hand. This reflects the contralateral nature of motor control and the complexity of motor execution. Right hand motor imagery, represented in Fig. 6b, shifts activation to the left hemisphere, within the corresponding region of the motor cortex. Strong activations are observed in Brodmann area 4, with additional involvement of Brodmann area 6, demonstrating motor planning and execution for the right hand's dexterous movements.

Feet motor imagery (Fig. 6c) engages the medial aspect of the motor cortex, particularly the areas responsible for the leg and foot regions of the motor homunculus. This task shows activation in the primary motor cortex (Brodmann area 4), near the longitudinal fissure, and extends into Brodmann area 6, which is essential for postural control and balance. For tongue motor imagery (Fig. 6d), activation is observed near the lateral sulcus in the lateral motor cortex. This region corresponds to the tongue area in the motor homunculus and shows strong activation in both Brodmann areas 4 and 6, indicating the coordination required for fine motor control involved in articulatory movements.

In summary, the beamforming results across motor imagery tasks demonstrate distinct activation patterns in the motor cortex that follow the somatotopic organization. The primary motor cortex (Brodmann area 4) consistently exhibits task-specific activations, while the premotor cortex (Brodmann area 6) plays a crucial role in motor planning. These findings highlight the interplay between motor execution and

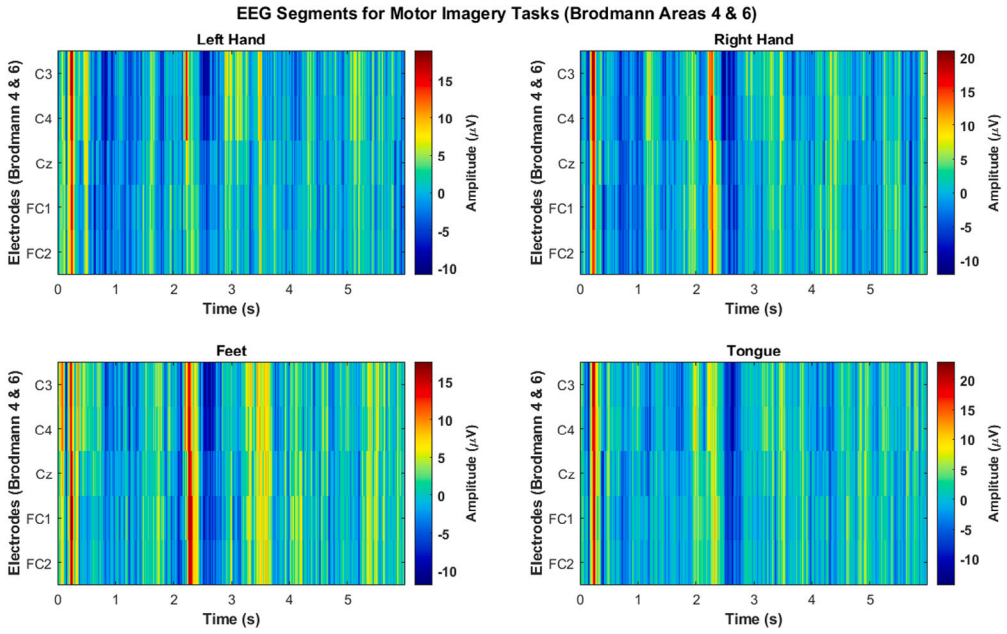

Fig. 5. EEG segments for four motor imagery tasks. Each subplot visualizes EEG activity across motor-related electrodes (C3, C4, Cz, FC1, FC2) associated with Brodmann Areas 4 and 6 during motor imagery of different movements. The tasks are arranged in a two-by-two layout: (top row, from left to right) Left Hand, Right Hand; (bottom row, from left to right) Feet, Tongue. The *x*-axis represents time from 0 to 6 s, covering the motor imagery phase. The *y*-axis indicates electrode placement, and the color scale represents EEG amplitude in microvolts (μV).

planning regions across the motor cortex. Moreover, the correlations between these areas, especially between Brodmann areas 4 and 6, emphasize how these regions work synergistically during different motor imagery tasks. The integration between motor execution and coordination becomes evident through the spatial–temporal dynamics observed in each task, providing novel insights into the functional connectivity underlying motor imagery.

3. Results and discussion

3.1. Performance of source localization methods in four-class EEG classification

In this section, we evaluate and compare the performance of various EEG classification methods using source localization techniques (Beamforming, MNE, and Dipole Fitting) with a deep ResNetCNN model against state-of-the-art sensor domain methods reported in the literature.

3.1.1. Classification with beamforming source localization

Table 2 presents the classification performance of the ResNetCNN model with Beamforming source localization across different subjects. The model achieved a high classification accuracy, ranging from **94.10%** for Subject 7 to **99.66%** for Subject 8. Beamforming consistently provided high accuracy across all subjects, with minimal variation, highlighting its robustness and reliability in isolating relevant EEG signals and enhancing spatial resolution. This consistent performance suggests that Beamforming effectively captures the direction of signal arrival, thereby significantly improving classification accuracy.

3.1.2. Classification with MNE source localization

Table 3 shows the classification performance using MNE source localization across different subjects. The accuracy achieved with MNE ranged from **97.22%** for Subject 8 to **99.65%** for Subjects 1, 3, 4, and 5. Although MNE provided substantial improvements in classification accuracy over sensor domain methods, there was noticeable variation

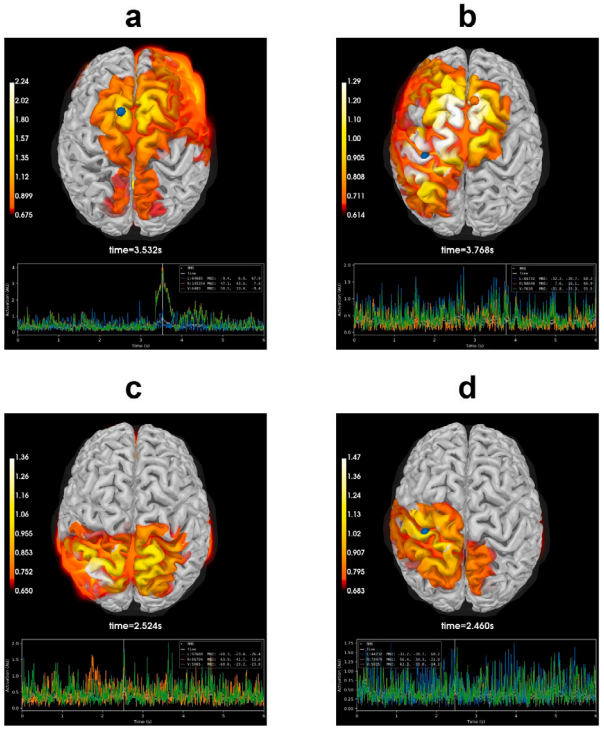

Fig. 6. (a) Left hand motor imagery showing activation in the right hemisphere, particularly in the primary motor cortex and premotor cortex. (b) Right hand motor imagery with activation in the left hemisphere, primarily engaging motor and premotor areas. (c) Feet motor imagery showing activation in the medial aspect of the motor cortex, near the longitudinal fissure, reflecting involvement in proximal limb control. (d) Tongue motor imagery with activation in the lateral motor cortex, near the lateral sulcus, indicating engagement of regions associated with fine motor control.

across subjects. This suggests that while MNE is effective in enhancing EEG data quality by estimating the sources of brain activity, it

Table 2
Performance of the deep ResNetCNN using beamforming source localization for EEG classification in Dataset 2a.

Subject	Accuracy (%)	Kappa	Precision (%)	Sensitivity (%)
1	99.65	0.995	99.66	99.65
2	98.96	0.986	98.98	98.96
3	98.61	0.981	98.63	98.61
4	99.31	0.991	99.32	99.31
5	97.92	0.972	97.97	97.92
6	99.31	0.991	99.31	99.31
7	94.10	0.921	94.41	94.10
8	**99.66**	**0.996**	**99.72**	**99.81**
9	98.61	0.981	98.65	98.61

Table 3
Performance of the deep ResNetCNN using MNE source localization for EEG classification in Dataset 2a.

Subject	Accuracy (%)	Kappa	Precision (%)	Sensitivity (%)
1	99.65	0.995	99.66	99.65
2	98.96	0.986	98.98	98.96
3	99.65	0.995	99.66	99.65
4	99.65	0.995	99.66	99.65
5	99.65	0.995	99.66	99.65
6	98.96	0.986	99.00	98.96
7	98.96	0.986	98.98	98.96
8	97.22	0.963	97.26	97.22
9	98.61	0.981	98.64	98.61

Table 4
Performance of the deep ResNetCNN using dipole fitting source localization for EEG classification in Dataset 2a.

Subject	Accuracy (%)	Kappa	Precision (%)	Sensitivity (%)
1	88.89	0.852	88.99	88.89
2	95.14	0.935	95.43	95.14
3	89.58	0.861	89.69	89.58
4	99.31	0.991	99.32	99.31
5	98.26	0.977	98.34	98.26
6	90.28	0.870	90.45	90.28
7	96.53	0.954	96.63	96.53
8	96.88	0.958	96.94	96.88
9	93.75	0.917	93.85	93.75

may not consistently capture all spatial details necessary for optimal performance, unlike Beamforming.

3.1.3. Classification with dipole fitting source localization

The results using Dipole Fitting for source localization are shown in Table 4. Dipole Fitting achieved an average accuracy ranging from **88.89%** for Subject 1 to **99.31%** for Subject 4. While this method provided a moderate improvement over several sensor domain methods, the performance was less consistent compared to Beamforming. This variability in accuracy suggests that Dipole Fitting, which models EEG sources as dipoles, may not always effectively isolate relevant brain signals for classification, leading to varying performance across subjects.

3.1.4. Comparison between sensor domain and source domain methods

Table 5 compares the classification accuracies of various state-of-the-art sensor domain methods with our proposed source localization methods using a deep ResNetCNN model. The Beamforming method achieved the highest average accuracy of **99.15%**, outperforming nearly all sensor domain methods, including TSCIR-Net [33]. Although TSCR-Net had the best performance overall, achieving an accuracy of 99.5%, Beamforming recorded a close performance, highlighting its effectiveness in enhancing EEG signal classification by accurately focusing on relevant brain signals and reducing noise and artifacts. Fig. 7 shows the confusion matrix for all subjects using Beamforming source localization, highlighting the classification accuracy across four motor imagery tasks.

Table 5
Comparison of classification accuracy of various methods in Dataset 2a. Beamforming, MNE, and dipole fitting combined with ResNetCNN are compared against state-of-the-art methods.

Proposed method	Dataset 2a (%)
FBGSP [34]	73.7
EEGNET [35]	74.5
ShallowConvNet [36]	74.31
DeepConvNet [36]	71.99
CWT + PSD + KMC [37]	89.3
CSP + SCNN [38]	64
DJDAN [39]	81.52
HS-CNN [40]	91.6
TCNET [33]	83.73
CNN with attentional mechanism + DA [33]	93.6
SW-LCR [41]	80
TCNetFusion [42]	83.73
MMBEEGSE [43]	82.87
E-CNNET [44]	89.25
TSCR-Net [45]	99.5
TSCIR-Net [45]	98
Beamforming + ResNetCNN	**99.15**
MNE + ResNetCNN	**83.49**
Dipole Fitting + ResNetCNN	**92.48**

In contrast, MNE and Dipole Fitting also showed improvements over many sensor domain methods, achieving accuracies of **83.49%** and **92.48%**, respectively. These methods, however, did not reach the performance levels of Beamforming, indicating that while they enhance EEG data quality, they may not isolate signals as effectively. This demonstrates the critical role of selecting appropriate source localization techniques to achieve the best classification outcomes.

The comparison between source domain and sensor domain methods clearly shows the advantages of using source localization techniques. The superior performance of Beamforming, combined with the ResNetCNN, suggests that source domain methods can substantially outperform sensor domain methods by providing enhanced spatial resolution and isolating relevant brain signals more effectively. This highlights the potential of source localization techniques in clinical and neurorehabilitation applications where precise detection of motor imagery tasks is crucial.

Overall, these findings emphasize the importance of source localization in improving EEG signal classification. By effectively isolating relevant brain activity and minimizing the impact of noise, source localization techniques like Beamforming enable deep learning models to achieve higher accuracy and more reliable performance in distinguishing between different motor imagery tasks. This is particularly important in applications requiring high precision, such as clinical diagnostics and brain–computer interface development.

3.2. Performance of source localization methods integrated with deep ResNet in Reach and Grasp Classification Tasks

In this study, we focused on decoding reach and grasp tasks from our EEG data in the sensor domain using a subject-specific classification approach. The process began by preprocessing the EEG signals for each subject individually, which involved applying a bandpass filter to isolate relevant frequency bands and using Independent Component Analysis (ICA) to remove artifacts. The cleaned signals were then used to extract features via power spectral density (PSD) using Welch's method, capturing the spectral characteristics of the EEG signals associated with different motor tasks.

A customized ResNet model was employed to classify the extracted features into specific reach and grasp tasks. The classification was conducted in the sensor domain, leveraging the spatial and spectral

Table 6
Performance of the proposed customized ResNet CNN in terms of recall, precision, F1-score, accuracy, and kappa for the reach and grasp classification tasks without source localization.

Subject	Accuracy (%)	Kappa (%)	Precision (%)	Recall (%)	F1 score (%)
1	50.56 ± 14.58	41.36 ± 17.01	53.21 ± 17.08	51.98 ± 15.12	48.62 ± 15.41
2	66.67 ± 7.45	60.42 ± 9.81	69.82 ± 10.01	67.00 ± 7.29	64.48 ± 8.04
3	56.67 ± 7.78	48.61 ± 9.74	61.84 ± 9.07	57.61 ± 8.16	55.25 ± 7.54
4	73.33 ± 8.16	68.31 ± 10.13	73.51 ± 11.01	73.24 ± 8.72	71.01 ± 10.09
5	44.44 ± 15.52	33.20 ± 19.05	45.18 ± 22.21	44.41 ± 16.13	41.12 ± 17.07
6	69.44 ± 11.45	63.81 ± 14.61	72.03 ± 15.51	69.26 ± 11.24	67.09 ± 14.81
7	70.00 ± 5.44	68.81 ± 7.06	73.98 ± 3.81	70.65 ± 5.07	70.45 ± 5.06
8	67.22 ± 8.41	61.02 ± 10.61	73.14 ± 9.11	67.22 ± 8.37	67.67 ± 8.19
9	70.56 ± 10.84	65.81 ± 13.08	73.98 ± 8.56	71.77 ± 11.06	68.74 ± 11.97
10	76.11 ± 3.56	75.09 ± 4.84	77.42 ± 3.56	76.99 ± 4.08	76.65 ± 4.42

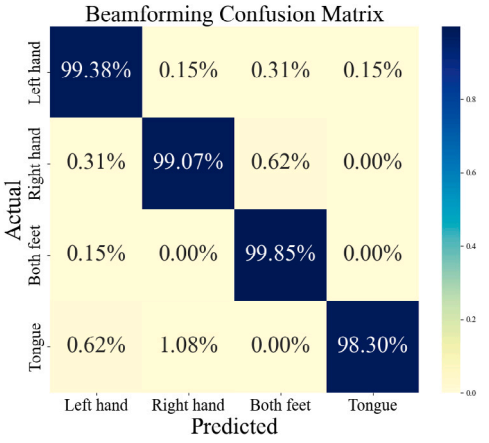

Fig. 7. Confusion matrix for all subjects using Beamforming source localization. This confusion matrix illustrates the classification performance across four motor imagery tasks: left hand, right hand, both feet, and tongue. The model achieved high performance, with overall accuracies above 99% for most classes and minimal misclassifications, demonstrating the effectiveness of Beamforming in enhancing EEG classification accuracy.

patterns present in the EEG signals. The model was trained separately for each subject using 10-fold cross-validation to ensure robust performance, capturing individual variations in EEG patterns. This subject-specific approach improved the accuracy of task decoding, demonstrating the effectiveness of using tailored EEG models for motor task classification.

3.2.1. Classification without source localization

The performance of the customized ResNet CNN without any source localization techniques is summarized in Table 6. The accuracy across subjects ranged from 44.44% to 76.11%, indicating that the classifier's ability to distinguish between the six grasp tasks varied significantly among subjects. The kappa scores, which measure the agreement between predicted and actual classes beyond chance, ranged from 33.20% to 75.09%. Precision values, indicating the proportion of positive identifications that were actually correct, varied from 45.18% to 77.42%. Recall values, reflecting the proportion of actual positives correctly identified, ranged from 44.41% to 76.99%, and F1-scores, which consider both precision and recall, ranged from 41.12% to 76.65%. These results highlight the challenges of decoding motor tasks directly from raw EEG signals without additional spatial information.

3.2.2. Classification with beamforming source localization

Beamforming significantly improved the classification performance. As detailed in Table 7, accuracy values ranged from 84.03% to 89.58%, showing a marked increase from the results without source localization. Precision values were much higher, between 86.69% and 91.35%, indicating a substantial enhancement in the classifier's ability to correctly identify positive instances. Recall values ranged from 84.03% to 89.58%, and F1-scores were consistently high, between 83.36% and 89.02%. These improvements underscore the effectiveness of beamforming in enhancing the spatial resolution of EEG data, leading to more reliable and accurate classifications.

3.2.3. Classification with MNE source localization

Using MNE for source localization also led to significant improvements, though less pronounced than beamforming. Table 8 shows that accuracy values ranged from 53.47% to 78.47%, with precision values between 56.98% and 79.83%. Recall values ranged from 53.47% to 78.47%, and F1-scores varied between 51.41% and 76.76%. These results indicate that MNE provided a meaningful boost to classification performance by minimizing the overall source strength while fitting the recorded data, though it was less effective than beamforming in isolating the relevant signals.

3.2.4. Classification with dipole fitting source localization

Dipole fitting yielded competitive accuracy scores, ranging from 50.69% to 72.92%, with precision values between 49.19% and 75.94%. Recall values ranged from 50.69% to 72.92%, and F1-scores were consistently moderate, between 46.93% and 71.40%, as represented in Table 9. These results suggest that dipole fitting provided a substantial improvement in classification performance, albeit less than beamforming. By modeling the EEG data as originating from a small number of dipoles, this method provided more focal source localization compared to distributed methods like MNE.

3.2.5. Comparison overall results between sensor domain and source domain methods

The comparison of classification performance across different conditions—beamforming, MNE, dipole fitting, and without source localization—provides valuable insights into the effectiveness of these techniques for EEG signal decoding. Table 10 summarizes the performance metrics of the deep CNN classifier for each method.

Among the source localization methods, beamforming achieved the best results with an Accuracy of 90.83% ±5.17%, Kappa of 89.00 ±6.20%, Precision of 91.08% ±5.14%, Average Recall of 90.83% ±5.17%, and F1 Score of 90.85% ±5.16%. These results highlight the ability of beamforming to isolate relevant neural activity more effectively, enhancing spatial resolution and improving classification accuracy. This technique's performance significantly surpasses that of MNE and dipole fitting, with MNE achieving an Accuracy of 84.10% ±11.36% and dipole fitting achieving 81.32% ±1.59%. By effectively reducing noise and dimensionality, beamforming leads to more precise decoding of motor tasks.

Compared to the performance of classifiers without source localization in the sensor domain, both ResNet-CNN (ICA + PSD) (52.61% ±2.29%) and TSCR-Net (56.39% ±3.82%) reveal the challenges of EEG classification when relying solely on sensor-level data. While TSCR-Net demonstrates a slight improvement over ResNet-CNN, achieving a nearly 4% higher accuracy, both models still perform significantly worse than beamforming (90.83% ±5.17%), which outperforms sensor-domain approaches by more than 34 percentage points.

Table 7
Performance of the proposed customized ResNet CNN for beamforming source localization in terms of recall, precision, F1-score, accuracy, and kappa for the reach and grasp classification tasks.

Subject	Accuracy (%)	Kappa (%)	Precision (%)	Recall (%)	F1 score (%)
1	89.58 ± 6.48	88.11 ± 8.56	91.15 ± 6.40	89.58 ± 6.48	89.02 ± 6.72
2	87.50 ± 11.37	85.08 ± 14.32	90.35 ± 8.12	87.50 ± 11.37	87.80 ± 10.31
3	88.89 ± 9.21	87.85 ± 11.27	90.35 ± 10.52	88.89 ± 9.21	88.11 ± 10.59
4	85.42 ± 9.19	82.01 ± 11.84	87.95 ± 9.02	85.42 ± 9.19	84.65 ± 9.73
5	85.42 ± 11.43	83.26 ± 14.65	87.43 ± 12.02	85.42 ± 11.43	84.92 ± 12.06
6	87.50 ± 5.38	85.98 ± 6.52	90.35 ± 5.02	87.50 ± 5.38	87.16 ± 5.38
7	88.89 ± 7.35	87.75 ± 9.62	91.35 ± 6.24	88.89 ± 7.35	88.50 ± 7.44
8	86.81 ± 9.60	84.28 ± 12.06	91.21 ± 5.41	86.81 ± 9.60	86.35 ± 9.49
9	88.89 ± 11.11	87.92 ± 13.31	90.66 ± 10.44	88.89 ± 11.11	88.40 ± 11.91
10	84.03 ± 11.60	81.35 ± 14.61	86.69 ± 11.10	84.03 ± 11.60	83.36 ± 12.76

Table 8
Performance of the proposed customized ResNet CNN for MNE source localization in terms of recall, precision, F1-score, accuracy, and kappa for the reach and grasp classification tasks.

Subject	Accuracy (%)	Kappa (%)	Precision (%)	Recall (%)	F1 score (%)
1	69.44 ± 17.35	63.84 ± 21.12	74.65 ± 16.46	69.44 ± 17.35	69.24 ± 16.63
2	68.75 ± 18.62	63.30 ± 22.84	73.37 ± 19.71	68.75 ± 18.62	68.36 ± 19.40
3	78.47 ± 17.44	74.62 ± 21.55	79.83 ± 21.32	78.47 ± 17.44	76.76 ± 19.81
4	75.69 ± 14.15	71.84 ± 17.32	76.91 ± 15.29	75.69 ± 14.15	74.13 ± 15.50
5	75.69 ± 16.88	71.42 ± 20.55	78.23 ± 17.20	75.69 ± 16.88	74.37 ± 18.58
6	53.47 ± 23.06	44.08 ± 28.31	56.98 ± 27.44	53.47 ± 23.06	51.41 ± 25.08
7	59.03 ± 24.68	51.42 ± 30.09	59.68 ± 24.55	59.03 ± 24.68	56.68 ± 25.08
8	64.58 ± 23.06	57.84 ± 28.82	63.64 ± 25.87	64.58 ± 23.06	62.14 ± 24.03
9	64.58 ± 17.77	57.31 ± 21.05	68.99 ± 16.03	64.58 ± 17.77	64.04 ± 17.50
10	73.61 ± 25.27	68.45 ± 30.61	75.03 ± 25.82	73.61 ± 25.27	72.92 ± 25.73

Table 9
Performance of the proposed customized ResNet CNN for dipole fitting source localization in terms of recall, precision, F1-score, accuracy, and kappa for the reach and grasp classification tasks.

Subject	Accuracy (%)	Kappa (%)	Precision (%)	Recall (%)	F1 score (%)
1	72.92 ± 12.25	68.01 ± 15.61	75.94 ± 11.51	72.92 ± 12.25	71.40 ± 12.42
2	70.14 ± 11.09	64.52 ± 13.48	74.62 ± 13.57	70.14 ± 11.09	69.53 ± 11.00
3	68.06 ± 11.37	62.30 ± 14.07	74.65 ± 11.18	68.06 ± 11.37	68.12 ± 11.14
4	60.42 ± 12.86	53.98 ± 15.41	63.51 ± 13.88	60.42 ± 12.86	59.07 ± 12.61
5	65.28 ± 10.67	58.84 ± 13.43	68.44 ± 11.41	65.28 ± 10.67	64.72 ± 10.94
6	56.94 ± 16.61	48.49 ± 20.11	57.74 ± 19.01	56.94 ± 16.61	55.46 ± 17.33
7	62.50 ± 21.65	55.41 ± 26.32	63.12 ± 22.68	62.50 ± 21.65	61.37 ± 22.12
8	50.69 ± 14.28	41.94 ± 17.01	49.19 ± 17.35	50.69 ± 14.28	46.93 ± 14.41
9	69.44 ± 8.78	63.44 ± 11.10	70.21 ± 11.78	69.44 ± 8.78	67.52 ± 9.58
10	64.58 ± 16.42	57.64 ± 20.82	64.02 ± 19.32	64.58 ± 16.42	62.39 ± 17.37

Table 10
Overall performance metrics of the proposed customized ResNet CNN for different source localization methods and without source localization.

Method	Accuracy (%)	Kappa (%)	Precision (%)	Recall (%)	F1 score (%)
Beamforming	**90.83 ± 5.17**	**89.00 ± 6.20**	**91.08 ± 5.14**	**90.83 ± 5.17**	**90.85 ± 5.16**
MNE	84.10 ± 11.36	80.92 ± 13.63	84.51 ± 11.11	84.10 ± 11.36	84.07 ± 11.36
Dipole fitting	81.32 ± 1.59	77.58 ± 1.91	81.62 ± 1.67	81.32 ± 1.59	81.31 ± 1.61
ResNet (Sensor domain)	52.61 ± 2.29	57.13 ± 2.75	48.10 ± 9.98	52.61 ± 2.29	56.94 ± 3.14
TSCR-Net (Sensor domain)	56.39 ± 3.82	47.67 ± 4.58	57.47 ± 3.56	56.39 ± 3.82	56.17 ± 3.69

This substantial performance gap highlights the limitations of sensor-space EEG analysis, where volume conduction effects, overlapping neural sources, and background noise reduce classification accuracy. In contrast, source localization techniques, such as beamforming, improve classification performance by isolating task-relevant brain activity at the cortical level, filtering out non-task-related signals, and reducing the influence of overlapping sources. The confusion matrix in Fig. 8 further illustrates how beamforming leads to a more precise classification of reach-and-grasp tasks, reinforcing its effectiveness compared to sensor-domain methods.

These findings also demonstrate that while deep learning models like TSCR-Net can slightly enhance EEG classification in the sensor domain, their performance remains heavily constrained by the raw input data quality. Without spatial filtering or source reconstruction, deep networks are unable to effectively compensate for the limitations of sensor-space EEG. The comparison emphasizes the critical role of source localization in EEG-based motor decoding and highlights beamforming as the most effective approach in this study.

3.3. Limitations and future work

Despite the high classification accuracy and robustness of the proposed method, some limitations remain. The dataset size is relatively small, which may impact generalizability. The computational complexity of source localization and deep learning models poses challenges for real-time applications. Inter-subject variability and EEG noise can affect beamforming performance. Future work should focus on real-time decoding and integrating additional modalities, such as EMG or fNIRS, to enhance motor task classification and system reliability.

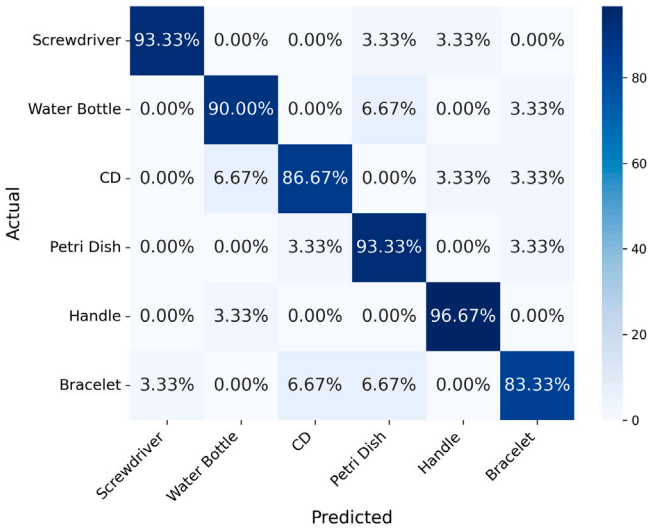

Fig. 8. Confusion matrix of the Beamforming classification results for different reach-and-grasp tasks. The matrix represents the percentage of correct and misclassified predictions for each class, where darker shades indicate higher classification accuracy.

4. Conclusion

In this study, we addressed the challenge of motor task classification using EEG data by integrating source localization techniques such as MNE, dipole fitting, and beamforming with a customized ResNet CNN. For the four-class motor imagery classification, beamforming achieved a peak accuracy of 99.15%, significantly outperforming sensor domain methods. In the six-class reach and grasp classification, beamforming yielded an accuracy of 90.83%, compared to 56.39% using the sensor domain approach (ICA + PSD + TSCR-Net). MNE and dipole fitting methods achieved accuracies of 84.10% and 81.32%, respectively. When comparing the best method, beamforming, against the sensor domain, we observed a substantial improvement in all metrics. Beamforming outperformed the sensor domain approach by a large margin, highlighting its ability to extract more relevant neural signals, leading to enhanced classification precision, recall, and F1-score. This study underscores the importance of source localization in EEG analysis. By utilizing these advanced techniques, we significantly improved the classification performance, showcasing the potential of combining source localization with deep learning for applications in brain–computer interfaces and neurorehabilitation.

CRediT authorship contribution statement

Sina Makhdoomi Kaviri: Writing – review & editing, Writing – original draft, Visualization, Validation, Software, Resources, Methodology, Formal analysis, Data curation. **Ramana Vinjamuri:** Writing – review & editing, Writing – original draft, Supervision, Resources, Project administration, Methodology, Investigation, Funding acquisition, Conceptualization.

Declaration of competing interest

The authors declare that they have no known competing financial interests or personal relationships that could have appeared to influence the work reported in this paper.

Acknowledgments

This research was funded by the National Science Foundation (NSF) CAREER Award, grant number IIS-2053498 and NSF IUCRC Phase II UMBC: BRAIN, grant number CNS-2333292.

Data availability

Data will be made available on request.

References

[1] J.R. Wolpaw, N. Birbaumer, D.J. McFarland, G. Pfurtscheller, T.M. Vaughan, Brain-computer interfaces for communication and control, Clin. Neurophysiol. 113 (6) (2002) 767–791.
[2] A. Biasiucci, B. Franceschiello, M.M. Murray, Electroencephalography, Curr. Biol. 29 (3) (2019) R80–R85.
[3] H. Zeng, A. Song, Optimizing single-trial EEG classification by stationary matrix logistic regression in brain–computer interface, IEEE Trans. Neural Netw. Learn. Syst. 27 (11) (2015) 2301–2313.
[4] H. Wang, C. Tang, T. Xu, T. Li, L. Xu, H. Yue, P. Chen, J. Li, A. Bezerianos, An approach of one-vs-rest filter bank common spatial pattern and spiking neural networks for multiple motor imagery decoding, IEEE Access 8 (2020) 86850–86861.
[5] H. Wang, T. Xu, C. Tang, H. Yue, C. Chen, L. Xu, Z. Pei, J. Dong, A. Bezerianos, J. Li, Diverse feature blend based on filter-bank common spatial pattern and brain functional connectivity for multiple motor imagery detection, IEEE Access 8 (2020) 155590–155601.
[6] H. Wang, T. Li, A. Bezerianos, H. Huang, Y. He, P. Chen, The control of a virtual automatic car based on multiple patterns of motor imagery BCI, Med. Biol. Eng. Comput. 57 (2019) 299–309.
[7] T. Xu, Z. Zhou, Y. Yang, Y. Li, J. Li, A. Bezerianos, H. Wang, Motor imagery decoding enhancement based on hybrid EEG-fNIRS signals, IEEE Access 11 (2023) 65277–65288.
[8] Y. Li, T. Xu, J. Li, F. Wan, H. Wang, Improved dilation CapsuleNet for motor imagery and mental arithmetic classification based on fNIRS, Brain- Appar. Commun.: J. Bacomics 3 (1) (2024) 2335886.
[9] M. Seeber, R. Scherer, G.R. Müller-Putz, EEG oscillations are modulated in different behavior-related networks during rhythmic finger movements, J. Neurosci. 36 (46) (2016) 11671–11681.
[10] G. Vecchiato, M. Del Vecchio, L. Ascari, S. Antopolskiy, F. Deon, L. Kubin, J. Ambeck-Madsen, G. Rizzolatti, P. Avanzini, Electroencephalographic time-frequency patterns of braking and acceleration movement preparation in car driving simulation, Brain Res. 1716 (2019) 16–26.
[11] P. Ofner, A. Schwarz, J. Pereira, D. Wyss, R. Wildburger, G.R. Müller-Putz, Attempted arm and hand movements can be decoded from low-frequency EEG from persons with spinal cord injury, Sci. Rep. 9 (1) (2019) 7134.
[12] B.J. Edelman, N. Johnson, A. Sohrabpour, S. Tong, N. Thakor, B. He, Systems neuroengineering: understanding and interacting with the brain, Engineering 1 (3) (2015) 292–308.
[13] A. Sohrabpour, B. He, Exploring the extent of source imaging: Recent advances in noninvasive electromagnetic brain imaging, Curr. Opin. Biomed. Eng. 18 (2021) 100277.
[14] B. Wodlinger, J.E. Downey, E.C. Tyler-Kabara, A.B. Schwartz, M.L. Boninger, J.L. Collinger, Ten-dimensional anthropomorphic arm control in a human brain-machine interface: difficulties, solutions, and limitations, J. Neural Eng. 12 (1) (2014) 016011.
[15] Y. Lee, Y. Huang, Generating target/non-target images of an RSVP experiment from brain signals by conditional generative adversarial network, in: Proc. 2018 IEEE EMBS Int. Conf. Biomedical & Health Informatics, BHI, 2018, pp. 182–185.
[16] F. Lotte, M. Congedo, A. Lécuyer, F. Lamarche, B. Arnaldi, A review of classification algorithms for EEG-based brain–computer interfaces, J. Neural Eng. 4 (2) (2007) R1.
[17] J. Pereira, P. Ofner, A. Schwarz, A.I. Sburlea, G.R. Müller-Putz, EEG neural correlates of goal-directed movement intention, Neuroimage 149 (2017) 129–140.
[18] X. Bi, X. Zhao, H. Huang, D. Chen, Y. Ma, Functional brain network classification for alzheimer's disease detection with deep features and extreme learning machine, J./Conf. Name 12 (2020) 513–527.
[19] Y. Roy, H. Banville, I. Albuquerque, A. Gramfort, T.H. Falk, J. Faubert, Deep learning-based electroencephalography analysis: a systematic review, J. Neural Eng. 16 (5) (2019) 051001.
[20] Z. Liu, B. He, fMRI–EEG integrated cortical source imaging by use of time-variant spatial constraints, Neuroimage 39 (3) (2008) 1198–1214.
[21] B. He, L. Yang, C. Wilke, H. Yuan, Electrophysiological imaging of brain activity and connectivity—challenges and opportunities, IEEE Trans. Biomed. Eng. 58 (7) (2011) 1918–1931.
[22] P. Ofner, A. Schwarz, J. Pereira, G.R. Müller-Putz, Upper limb movements can be decoded from the time-domain of low-frequency EEG, PloS One 12 (8) (2017) e0182578.
[23] L.R. Hochberg, D. Bacher, B. Jarosiewicz, N.Y. Masse, J.D. Simeral, J. Vogel, S. Haddadin, J. Liu, S.S. Cash, P. Van Der Smagt, et al., Reach and grasp by people with tetraplegia using a neurally controlled robotic arm, Nature 485 (7398) (2012) 372–375.

[24] N. Mammone, C. Ieracitano, F.C. Morabito, A deep CNN approach to decode motor preparation of upper limbs from time–frequency maps of EEG signals at source level, Neural Netw. 124 (2020) 357–372.
[25] C. Ieracitano, N. Mammone, A. Hussain, F.C. Morabito, A novel explainable machine learning approach for EEG-based brain-computer interface systems, Neural Comput. Appl. 34 (14) (2022) 11347–11360.
[26] D. Pei, P. Olikkal, T. Adali, R. Vinjamuri, Reconstructing synergy-based hand grasp kinematics from electroencephalographic signals, Sensors 22 (14) (2022) 5349.
[27] C. Brunner, R. Leeb, G. Müller-Putz, BCI competition 2008–graz data set A, 2024, http://dx.doi.org/10.21227/katb-zv89, IEEE Dataport, [Online]. Available.
[28] S. Haufe, Y. Huang, L.C. Parra, A highly detailed FEM volume conductor model based on the ICBM152 average head template for EEG source imaging and TCS targeting, in: Conf. Proc. IEEE Eng. Med. Biol. Soc., vol. 2015, 2015, pp. 5744–5747.
[29] R. Grech, T. Cassar, J. Muscat, K.P. Camilleri, S.G. Fabri, M. Zervakis, P. Xanthopoulos, V. Sakkalis, B. Vanrumste, Review on solving the inverse problem in EEG source analysis, J. Neuroeng. Rehabil. 5 (2008) 1–33.
[30] S. Asadzadeh, T.Y. Rezaii, S. Beheshti, A. Delpak, S. Meshgini, A systematic review of EEG source localization techniques and their applications on diagnosis of brain abnormalities, J. Neurosci. Methods 339 (2020) 108740.
[31] M. Grosse-Wentrup, C. Liefhold, K. Gramann, M. Buss, Beamforming in non-invasive brain–computer interfaces, IEEE Trans. Biomed. Eng. 56 (4) (2009) 1209–1219.
[32] R. Oostenveld, P. Fries, E. Maris, J.-M. Schoffelen, FieldTrip: Open source software for advanced analysis of MEG, EEG, and invasive electrophysiological data, Comput. Intell. Neurosci. 2011 (2011) 156869.
[33] Y.K. Musallam, N.I. AlFassam, G. Muhammad, S.U. Amin, M. Alsulaiman, W. Abdul, H. Altaheri, M.A. Bencherif, M. Algabri, Electroencephalography-based motor imagery classification using temporal convolutional network fusion, Biomed. Signal Process. Control. 69 (2021) 102826.
[34] K.K. Ang, Z.Y. Chin, C. Wang, C. Guan, H. Zhang, Filter bank common spatial pattern algorithm on BCI competition IV datasets 2a and 2b, Front. Neurosci. 6 (2012) 39.
[35] V.J. Lawhern, A.J. Solon, N.R. Waytowich, S.M. Gordon, C.P. Hung, B.J. Lance, EEGNet: a compact convolutional neural network for EEG-based brain–computer interfaces, J. Neural Eng. 15 (5) (2018) 056013.
[36] R.T. Schirrmeister, J.T. Springenberg, L.D.J. Fiederer, M. Glasstetter, K. Eggensperger, M. Tangermann, F. Hutter, W. Burgard, T. Ball, Deep learning with convolutional neural networks for EEG decoding and visualization, Hum. Brain Mapp. 38 (11) (2017) 5391–5420.
[37] C. Kim, J. Sun, D. Liu, Q. Wang, S. Paek, An effective feature extraction method by power spectral density of EEG signal for 2-class motor imagery-based BCI, Med. Biol. Eng. Comput. 56 (2018) 1645–1658.
[38] X. Zhu, P. Li, C. Li, D. Yao, R. Zhang, P. Xu, Separated channel convolutional neural network to realize the training free motor imagery BCI systems, Biomed. Signal Process. Control. 49 (2019) 396–403.
[39] X. Hong, Q. Zheng, L. Liu, P. Chen, K. Ma, Z. Gao, Y. Zheng, Dynamic joint domain adaptation network for motor imagery classification, IEEE Trans. Neural Syst. Rehabil. Eng. 29 (2021) 556–565.
[40] G. Dai, J. Zhou, J. Huang, N. Wang, HS-CNN: a CNN with hybrid convolution scale for EEG motor imagery classification, J. Neural Eng. 17 (1) (2020) 016025.
[41] E. Lashgari, J. Ott, A. Connelly, P. Baldi, U. Maoz, An end-to-end CNN with attentional mechanism applied to raw EEG in a BCI classification task, J. Neural Eng. 18 (4) (2021) 0460e3.
[42] P. Gaur, H. Gupta, A. Chowdhury, K. McCreadie, R.B. Pachori, H. Wang, A sliding window common spatial pattern for enhancing motor imagery classification in EEG-BCI, IEEE Trans. Instrum. Meas. 70 (2021) 1–9.
[43] G.A. Altuwaijri, G. Muhammad, H. Altaheri, M. Alsulaiman, A multi-branch convolutional neural network with squeeze-and-excitation attention blocks for EEG-based motor imagery signals classification, Diagnostics 12 (4) (2022) 995.
[44] M. Kaur, R. Upadhyay, V. Kumar, E-CNNet: Time-reassigned multisynchrosqueezing transform-based deep learning framework for MI-BCI task classification, Int. J. Imaging Syst. Technol. 33 (4) (2023) 1406–1423.
[45] H. Mirzabagherian, M.B. Menhaj, A.A. Suratgar, N. Talebi, M.R.A. Sardari, A. Sajedin, Temporal-spatial convolutional residual network for decoding attempted movement related EEG signals of subjects with spinal cord injury, Comput. Biol. Med. 164 (2023) 107159.